

Article

# Combustion Chamber Optimization for Dual-Fuel Biogas–Diesel Co-Combustion in Compression Ignition Engines

Stefano Caprioli \* , Antonello Volza, Francesco Scignoli , Tommaso Savioli, Enrico Mattarelli   
and Carlo Alberto Rinaldini 

Department of Engineering ‘Enzo Ferrari’, University of Modena and Reggio Emilia, Via Pietro Vivarelli 10, 41125 Modena, Italy

\* Correspondence: stefano.caprioli@unimore.it

**Abstract:** Micro-cogeneration with locally produced biogas from waste is a proven technique for supporting the decarbonization process. However, the strongly variable composition of biogas can make its use in internal combustion engines quite challenging. Dual-fuel engines offer advantages over conventional SI and diesel engines, but there are still issues to be addressed, such as the low-load thermodynamic efficiency and nitrogen oxide emissions. In particular, it is highly desirable to reduce NO<sub>x</sub> directly in the combustion chamber in order to avoid expensive after-treatment systems. This study analyzed the influence of the combustion system, especially the piston bowl geometry and the injector nozzle, on the performance and emissions of a dual-fuel diesel–biogas engine designed for micro-cogeneration (maximum electric power: 50 kW). In detail, four different cylindrical piston bowls characterized by radii of 23, 28, 33 and 38 mm were compared with a conventional omega-shaped diesel bowl. Moreover, the influence of the injector tip position and the jet tilt angle was analyzed over ranges of 2–10 mm and 30–120°, respectively. The goal of the optimization was to find a configuration that was able to reduce the amount of NO<sub>x</sub> while maintaining high values of brake thermal efficiency at all the engine operating conditions. For this purpose, a 3D-CFD investigation was carried out by means of a customized version of the KIVA-3V code at both full load (BMEP = 8 bar, 3000 rpm, maximum brake power) and partial load (BMEP = 4 bar, 3000 rpm). The novelty of the study consisted of the parametric approach to the problem and the high number of investigated parameters. The results indicated that the standard design of the piston bowl yielded a near-optimal trade-off at full load between the thermodynamic efficiency and pollutant emissions; however, at a lower load, significant advantages could be found by designing a deeper cylindrical bowl with a smaller radius. In particular, a new bowl characterized by a radius of 23 mm was equivalent to the standard one at BMEP = 8 bar, but it yielded a NO<sub>x</sub>-specific reduction of 38% at BMEP = 4 bar with the same value of BTE.

**Keywords:** biogas; micro-cogeneration; dual fuel; bowl optimization; injection; 3D-CFD analysis



**Citation:** Caprioli, S.; Volza, A.; Scignoli, F.; Savioli, T.; Mattarelli, E.; Rinaldini, C.A. Combustion Chamber Optimization for Dual-Fuel Biogas–Diesel Co-Combustion in Compression Ignition Engines. *Processes* **2023**, *11*, 1113. <https://doi.org/10.3390/pr11041113>

Academic Editor: Weizhong Dai

Received: 28 February 2023

Revised: 17 March 2023

Accepted: 1 April 2023

Published: 5 April 2023



**Copyright:** © 2023 by the authors. Licensee MDPI, Basel, Switzerland. This article is an open access article distributed under the terms and conditions of the Creative Commons Attribution (CC BY) license (<https://creativecommons.org/licenses/by/4.0/>).

## 1. Introduction

The use of self-produced biogas (BG) in micro-cogeneration (production of electrical energy and heat up to 50 kW of electric power) can be a fundamental enabler of a clean and efficient energy distribution system, i.e., a “smart grid” [1,2]. This technology is particularly interesting for small- and medium-sized agricultural companies, whose activities include raising cattle, cultivation of fields for feeding the animals, and production of milk and cheese. Such a farm can also produce a sufficient quantity of BG from cattle manure, agricultural wastes and specific crops. The investigation made by Havrysh et al. [3] showed that cogeneration plants fuelled by biomass provide the best circular economy indicators, with a carbon dioxide (CO<sub>2</sub>) reduction of up to 393 kg per ton of seed.

Furthermore, according to the calculations made by Kalinichenko et al. [4] regarding the price of alternative fuels for transport, the best one seems to be natural gas (NG), which has combustion characteristics that are very similar to BG. In this scenario, it should be convenient for a small-to-medium farm to adopt an internal combustion engine running on self-produced BG for micro-cogeneration. In fact, the farm could become almost completely energy-independent, saving money and greatly reducing its carbon footprint, as demonstrated, for instance, by Legrottaglie et al. [5].

BG can be flexibly produced by both continuous and batch anaerobic digestion, depending on the available feedstock [6].

One of the main challenges related to the employment of BG in internal combustion engines is the variability of its composition [7]. Table 1 shows the main constituents and their ranges of variation [8].

**Table 1.** BG composition and properties.

Constituent	Range
Methane (CH <sub>4</sub> ) [vol%]	30–73
Carbon dioxide (CO <sub>2</sub> ) [vol%]	20–40
Nitrogen (N <sub>2</sub> ) [vol%]	5–40
Hydrogen (H <sub>2</sub> ) [vol%]	1–3
Oxygen (O <sub>2</sub> ) [vol%]	0–5
Physical Property	
Density [kg/m <sup>3</sup> ]	0.65–0.91
Octane number [-]	130
Auto-ignition temperature [°C]	632–813
Lower heating value [MJ/Nm <sup>3</sup> ]	10–25

A particularly critical aspect of the BG composition is the amount of CO<sub>2</sub>, which affects the laminar flame speed [9]. A large fraction of CO<sub>2</sub> can greatly reduce it, making it difficult to obtain regular combustion in spark ignition (SI) engines. Some researchers [10,11] also demonstrated that the CO<sub>2</sub> concentration has an influence on the knocking tendency: the lower the amount of CO<sub>2</sub>, the higher the risk of knocking. As a result, SI engines require a sophisticated electronic control system to reduce cycle-by-cycle variation and prevent knocking.

Moreover, the fuel conversion efficiency of this type of engine is limited by some technical aspects: relatively low thermodynamic efficiency due to the low compression ratio, throttling losses at partial load and non-complete combustion due to the necessity of running on rich mixtures at some operating conditions.

By using compression ignition (CI) rather than SI, the previous issues can be fixed or at least mitigated: knocking is no longer a problem, the compression ratio can be increased considerably, combustion is always lean and the load can be controlled without throttling the flow. BG can be injected within the intake manifold, as on a standard SI engine, and combustion will be started by the injection of a small quantity of diesel fuel. This concept, which is referred to as reactivity-controlled compression ignition (RCCI) or dual-fuel (DF) combustion, was well assessed and investigated by several experimental and numerical studies that considered different fuels [12–15]. In comparison to an SI engine delivering the same brake power, a DF engine typically has higher fuel conversion efficiency, which is comparable to or even better than conventional diesels. On the other hand, pollutant emissions (CO, HC, NO<sub>x</sub> and soot) require a dedicated analysis [8,16]. While carbon monoxide (CO) and unburnt hydrocarbon (HC) can be eliminated using a simple oxidation catalyst, the formation of nitrogen oxides (NO<sub>x</sub>) and soot must be limited within the cylinders in order to avoid the installation of a complex and expensive after-treatment system.

In their detailed review, Wei et al. [17] reported that a DF engine is almost smokeless in low-speed and low-load conditions.

NO<sub>x</sub> control is particularly critical since any measure that is taken to reduce the pollutant tends to worsen the thermodynamic efficiency of the engine and vice versa. Moreover, as the engine load increases from low to medium, the control of RCCI combustion becomes more and more difficult [18]: the cylinder pressure tends to rise abruptly, generating high peaks and gradients, which increases the combustion noise and the risk of mechanical failures. Therefore, to operate at medium-to-high loads, a high amount of exhaust gas recirculation (EGR) and/or low compression ratios (CRs) are needed at the expense of the thermodynamic efficiency of the engine [19,20].

To fix the abovementioned problem, some researchers [8] proposed the use of indirect injection (IDI) diesel engines. In DF operations blends, NO<sub>x</sub> emissions strongly decrease (about 70% lower) in comparison to the operations on a single fuel. Furthermore, the soot and CO<sub>2</sub> emissions are lower. Conversely, the concentrations of CO and HC were found to be considerably higher than those corresponding to the single-fuel operations. These emissions can be easily managed using an oxidation catalyst, but the brake thermal efficiency (BTE) of an IDI engine is lower than that of the DI version.

The development of a clean and efficient combustion system for a DF engine is typically based on the optimization of the composition of the premixed charge (air, BG and burnt gas) and the calibration of the injection strategy [21,22]. To reduce the cost, no modification is made to the combustion chamber geometry or the injector of the original diesel engine. Unfortunately, a combustion chamber and an injector designed for standard diesel combustion are not ideal for a DF application for the reasons that will be discussed in the next section.

Other studies on RCCI combustion were focused on the different fuels that can be coupled to diesel fuel, such as DME/CH<sub>4</sub> [23], methanol [24] and gasoline [25]. These studies demonstrated that the optimization of the diesel injection strategy is the key to decreasing NO<sub>x</sub> and HC emissions over a wide range of DF configurations and operating conditions.

The non-condensable gas deriving from the pyrolysis of *Albizia odoratissima*, which is mainly composed of hydrogen and carbon dioxide, along with lower amounts of carbon monoxide and methane, may also be used as low-reactivity fuel in RCCI combustion [26]. Ali et al. found that the addition of 1-octanol as a C8 oxygenate to biodiesel extracted from waste cooking oil can effectively mitigate smoke and deliver optimal emissions and performance characteristics on a diesel engine with a compression ratio of 19:1. The optimized blend named D80WCOME15-OCT5, with a 10% EGR rate, was found to reduce the smoke opacity by 29.4%, increase NO<sub>x</sub> emissions by 4.07% and improve the BTE by 1.22% [27].

Ramesh et al. performed an extensive experimental campaign on three PJOME–diesel blends: 10%, 20% and 30% (B10, B20 and B30); the engine compression ratio was varied from 16:1 to 19:1 and the fuel injection pressure (FIP) was varied from 400 to 600 bar. B20 with an FIP of 600 bar and a CR of 16 provided the highest value of the BTE (33.2%) with a low amount of UHC [28].

Regarding the design of the combustion chamber for RCCI combustion, when using methanol and gasoline as low-reactivity fuel, Dempsey et al. [29] proposed a shallow piston bowl and a flat cylinder head. For both gasoline/diesel fuel and methanol/diesel fuel operation, it was found that the modified piston yielded a 2–4% improvement in terms of the gross indicated efficiency.

Gianetti et al. [30] performed a CFD analysis to evaluate the advantages and disadvantages of different combustion chamber designs in an NG-fuelled SI engine, operating at different loads and speeds. Despite the good accuracy of the numerical model, as demonstrated by the agreement between the simulation and experiments, no significant improvements in terms of combustion efficiency could be found. Lee et al. [31] modified the combustion chamber geometry of a diesel engine to operate in DF gasoline–diesel mode. They also analyzed the influence of the diesel start-of-injection (SOI) timing on the spray tip penetration and ignition delay. The modified combustion chamber was similar to the

original design but less deep; the reduction in the gross indicated specific fuel consumption (gISFC) was 14%.

Some recent articles analyzed DF combustion with BG as low-reactivity fuel [32,33], finding that the highest efficiency conditions corresponded to high engine speeds and loads and that the CO<sub>2</sub> concentration in the BG composition strongly affected the NO<sub>x</sub> emissions.

Another experimental study on DF BG–diesel combustion in a single-cylinder engine operating at low, medium and high loads was presented in [34]. Thanks to the optimization of the injection and ignition strategy, NO<sub>x</sub> emissions were lowered by up to 57% in comparison to the original diesel engine. However, it was observed that the HC emissions tended to increase. Moreover, at low loads, the lean BG–air mixture caused flame quenching.

The study presented in this article was focused on the combustion process of a dual-fuel diesel–biogas engine at two different loads. The purpose was to analyze, by means of 3D-CFD simulations, the influence of the most important parameters related to the combustion chamber design, in particular, the bowl shape, the injector tip position and the tilt angle of the diesel spray. The range of variation of the analyzed parameters is shown below:

- Radius of the piston bowl: 23, 28, 33 and 38 mm;
- Axial position of the injector tip: from 2 to 10 mm in steps of 1 mm;
- Tilt angle from 30° to 120° in steps of 15°.

For each configuration, the diesel injection strategy was also analyzed.

The study was carried out on a CI, four-cylinder, 2.8 L turbocharged common rail engine that was modified to run in DF mode with BG. Different from the majority of existing DF power plants, the “donor” was a commercial light-duty engine with relatively high specific power. In a previous work [5], the engine was adapted for micro-cogeneration use, achieving an electric power rate of 50 kW at 3000 rpm without any modification to the original combustion chamber and injector. The study was supported by a comprehensive experimental campaign carried out on a four-cylinder prototype and via numerical simulation (1D- and 3D-CFD analyses). In comparison to a typical SI engine, the main advantages of the DF engine were found to be a 20% higher BTE (due to the higher efficiency of the thermodynamic cycle and lower thermal and pumping losses) and 20% lower CO<sub>2</sub> emissions (due to the lower BG consumption). The main disadvantage was the poor combustion efficiency at low load that led to a low BTE and high HC and CO emissions: at BMEP < 2 bar, the engine operations must be switched to normal diesel combustion to avoid this problem. Therefore, the goal of the current study was to develop a new combustion system that was able to run in an efficient and clean way at both full and partial loads.

The novelty of this study, in comparison to other works found in the literature on the same topic, consists of the parametric approach to the problem and the very high number of investigated parameters.

## 2. Materials and Methods

### 2.1. Combustion System Design

The combustion chamber geometry of a diesel engine is designed to promote air–fuel mixing during the last phase of the injection process. For this purpose, the axially symmetric piston bowl is characterized by a typical “omega” shape, which helps to increase the strength of the swirl motion during the last part of the compression stroke; moreover, the cylinder head is flat to generate a radial flow (squish) around the top dead center (TDC).

Unfortunately, this design is not ideal for DF combustion, where the diffusive phase is almost negligible in comparison to the premixed phase (several flame fronts generated by the ignition of a small amount of high-reactivity fuel propagate within a homogeneous and lean mixture of low-reactivity fuel and air). The premixed combustion mode needs a high turbulence intensity (more than high values of swirl) to increase the surface area of the flame front, and thus, the burn rate. Another fundamental aspect is the compactness of the combustion chamber: the shorter the average flame path, the better it is for the completeness of the combustion process. Moreover, a compact chamber is generally characterized

by high values of the volume-to-surface-area ratio, which reduces HC emissions, minimizes the heat losses through the chamber walls, and thus, improves the efficiency of the engine cycle.

An ideal design for a DF combustion chamber involves both the cylinder head and the piston bowl. However, the modification of the cylinder head does not appear as a practical proposition since it would require a complete revision of the engine layout. Conversely, a brand new design of the piston bowl seems more feasible.

In order to obtain some theoretical guidelines for the design of a DF combustion chamber, we considered a simple cylindrical bowl with a flat cylinder head. The axis of the bowl corresponded with the cylinder axis. Moreover, the injection was axially symmetric. It was also assumed that the compression ratio and the squish clearance (minimum distance between the piston and cylinder head) were constant. Therefore, as the depth of the cylindrical bowl increased, the following trends could be observed:

- The squish velocity increased [35];
- The heat transfer area of the chamber increased.

These two trends had opposite effects. The higher the squish intensity, the higher the turbulence intensity, thanks to the interaction between the radial flow and the swirl motion within the bowl, which generates a dissipation of kinetic energy [36]. Moreover, the centrifugal radial motion after TDC speeds up the propagation of the flame fronts. On the other hand, the larger the surface area associated with the strong turbulence, the larger the heat losses.

Supposing that ignition occurs close to the injector nozzle, the compactness of the combustion chamber can be assessed by means of the maximum distance between the injector and the wall of the piston bowl at TDC. Neglecting the motion of the piston during the combustion process, this parameter corresponds to the maximum distance traveled by the flame front to sweep the whole chamber. Such a distance  $l$  can be expressed as

$$l = \sqrt{h^2 + \frac{d^2}{4}} \quad (1)$$

where  $h$  is the depth of the bowl and  $d$  is its diameter.

The hypothesis of the constant volume of the bowl (to maintain the same compression ratio) yields

$$\frac{d^2}{4} = \frac{V_{bowl}}{\pi h} \quad (2)$$

where  $V_{bowl}$  is the volume of the bowl.

Therefore, combining Equations (1) and (2):

$$l = \sqrt{h^2 + \frac{V_{bowl}}{\pi h}} \quad (3)$$

The depth of the bowl that minimizes the parameter  $l$  is

$$h = \sqrt[3]{\frac{V_{bowl}}{2\pi}} \quad (4)$$

In conclusion, the discussion above demonstrates that the design of a piston bowl for a DF combustion presents conflicting issues; therefore, it must be supported by accurate numerical analyses and/or experiments. Moreover, the outcome strongly depends on the goals of the optimization, as well as on the constraints of the problem, in particular, the compression ratio, squish clearance, bore, et cetera.

## 2.2. The 3D-CFD Code

For the numerical analysis of the DF combustion process on alternative combustion systems, a customized version of the 3D-CFD KIVA-3V code was used [37]. The code solves the conservation equations for evaporating fuel sprays, coupled with the 3-dimensional computational fluid dynamics (3D-CFD) equations of compressible, multi-component, reactive gases in an engine cylinder with an arbitrarily shaped piston geometry. As listed

in Table 2, the RNG  $k-\epsilon$  model was used as the turbulence model since it represents the standard for in-cylinder flows of internal combustion engines, while the spray atomization was modeled using the Kelvin–Helmholtz/Rayleigh–Taylor (KH-RT) instability model. For the simulation of the DF combustion process, two coupled models were used: the “conventional” partially stirred reactor (PaSR) and the turbulent flame closure (TFC). The code also includes a detailed chemical kinetic mechanism for NG/BG and diesel fuel that was validated on the basis of experimental measurements of ignition delay times in a shock tube and flame propagation speed [38].

**Table 2.** Main models used for the 3D-CFD engine modeling.

Turbulence model	RNG $k-\epsilon$ model
Breakup model	Hybrid KH-RT model
Droplet collision model	Droplet trajectories
Combustion	PaSR coupled with chemical kinetics
Flame propagation	TFC/premix code for aspirated fuel
Fuel composition	Natural gas/diesel oil surrogate

The fuels used in the analysis were modeled as follows:

- NG was a 3-component mixture of CH<sub>4</sub> (95 vol%), ethane (C<sub>2</sub>H<sub>6</sub>, 4 vol%) and propane (C<sub>3</sub>H<sub>8</sub>, 1 vol%).
- BG was a 3-component mixture of CH<sub>4</sub> (65 vol%), CO<sub>2</sub> (30 vol%) and N<sub>2</sub> (5 vol%).
- Diesel fuel was represented by the diesel oil surrogate (DOS) model, in which the liquid fuel properties are the same as real diesel fuel (with an equivalent chemical formula corresponding to C<sub>14</sub>H<sub>28</sub>), while the fuel vapor is made up of a 70/30 vol% blend of n-heptane (C<sub>7</sub>H<sub>16</sub>) and toluene (C<sub>7</sub>H<sub>8</sub>) [39]. The aliphatic hydrocarbon represents the main component of the blend since its cetane number (CN), equal to 56, is similar to the one of real diesel fuel. Considering that the CN of toluene is equal to about 9, the calculated CN of the DOS model is about 47 [40]. The single-component liquid fuel model is assumed to decompose into the two-component fuel vapor model through the following pyrolysis reaction:



This approach is due to the fact that the oxidation scheme of real diesel fuel is not known. The chemical kinetic mechanism includes 81 species and 421 reactions.

The version of the KIVA-3V code used for the study was already applied by the authors to the analysis of different diesel and DF engines, and the results of the calculations were always found to be in good agreement with experiments, as reported in [5,41–43].

The computational grid was built using the K3PREP pre-processor of the KIVA-3V package. A 60° sector grid with proper periodic boundary conditions was considered to exploit the axial symmetry of the combustion chamber and the homogeneous spatial distribution of the 6 holes of the diesel injector. In building the grid, a characteristic cell size of 0.8 mm was used and a minimum of four cell layers was enforced in the squish region at the TDC. As demonstrated by previous analyses, these meshing criteria guarantee a good compromise between accuracy and computational cost [43].

In this study, the characteristic cell size was varied between 0.5 and 1.7 mm. Based on the most important outputs of the simulations (total heat released) and the computational cost, the best global cell size was determined. The computational grid built for the study is shown in Figure 1. It was made up of approximately 80,000 cells at the bottom dead center (BDC) and about 24,000 cells at the TDC. This was due to the fact that, as the piston moved from the BDC to TDC (and vice versa), cells were compressed (stretched) up to the point where a cell layer was removed (added).

The combustion simulations were carried out between the intake valve closing (IVC, −130 °CA aTDC) and exhaust valve opening (EVO, 112 °CA aTDC). Initial conditions, such as pressure, temperature, trapped mass and charge composition, were directly obtained

from the experimental data. The initial flow field was imposed as a rigid vortex around the cylinder axis; its intensity (swirl ratio equal to 1.8) was calculated using a previous 3D-CFD intake stroke simulation.

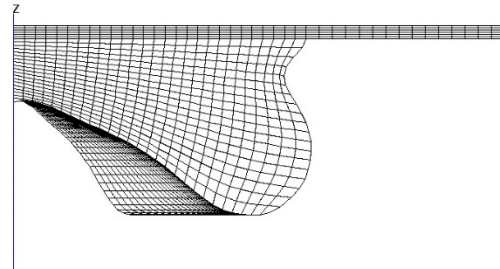


**Figure 1.** Computational grid at the TDC.

### 2.3. Numerical Model and Validation

The reference engine used for the analysis was an automotive high-speed direct-injection (HSDI) diesel engine manufactured by FCA–VM Motori, whose main characteristics are listed in Table 3. The engine was modified by the authors to run in DF NG–diesel fuel mode, and a comprehensive experimental campaign was carried out to optimize the DF combustion over a wide range of operating points. Based on the abovementioned experimental activity, a 3D-CFD model of the combustion system was built and validated. For the sake of brevity, the model validation was reported in this paper only for the micro-generation peak power operating point (55.6 kW, 3000 rpm, 8 bar BMEP), which was characterized by a reduction in the diesel fuel mass equal to 80% with respect to the corresponding diesel case. The main engine parameters used for the validation of the numerical model are listed in Table 4. Figure 2a reports the comparison between the simulation and experimental results in terms of the in-cylinder pressure and rate of heat release (RoHR). As can be noticed, the numerical results were in reasonable agreement with the experiments. For a full description of the results of the experimental campaign and the whole validation of the numerical model, the reader is referred to [5,41,43].

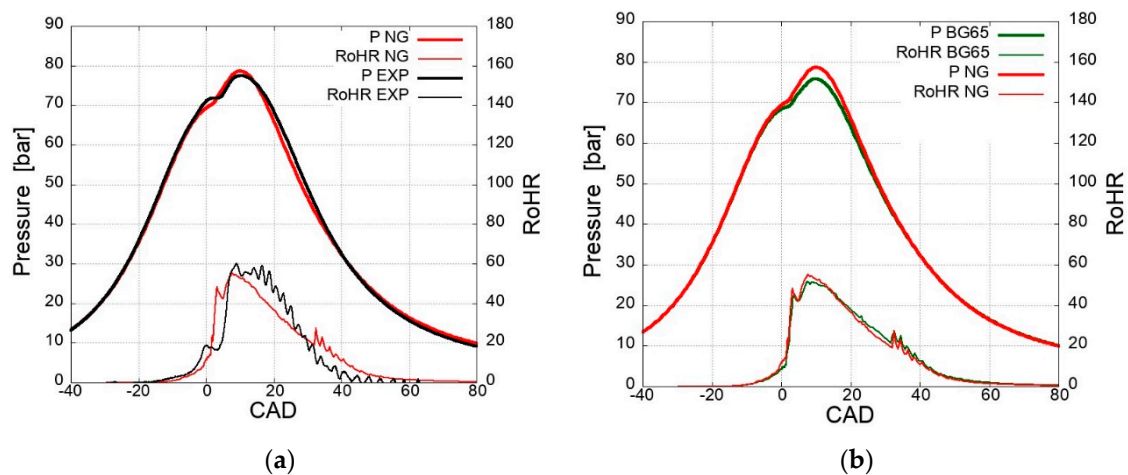
After the validation, the model was employed for the simulation of the co-combustion of diesel fuel and BG. In order to take into account the BG composition, the initial composition of the premixed charge was recalculated. The amount of CH<sub>4</sub> in the BG was chosen to have the same energy content as the NG case. Table 5 shows the main operating point features, while Figure 2b shows the comparison between the combustion of NG and BG. It can be observed that despite having the same amount of available potential energy, the scenario involving BG exhibited slightly lower pressure. This can be attributed to a slower combustion process resulting from a lower quantity of air present.

**Table 3.** Main technical data of the reference diesel engine.

Engine type	HSDI 4-S diesel, EURO IV
Cylinders	4 in-line
Total displacement [L]	2.78
Bore × stroke [mm]	94 × 100
Compression ratio	17.5:1
No. of valves per cylinder	4
Air metering	Turbocharger with VGT + intercooler
Injection system	Common rail
Number of injector holes	6
Injector hole diameter [mm]	0.153

**Table 4.** Main engine parameters of the experimental validation case.

Trapped mass [mg/cycle/cyl]	918.63
Air mass [mg/cycle/cyl]	801.90
NG mass [mg/cycle/cyl]	24.86
Diesel fuel mass [mg/cycle/cyl]	6.62
Diesel fuel injection pressure [bar]	1050
Diesel fuel pilot SOI [°CA AFTDC]	−21.66
Diesel fuel pilot duration [°CA]	3.25
Diesel fuel pre SOI [°CA AFTDC]	−13.92
Diesel fuel pre-duration [°CA]	3.60
Diesel fuel main SOI [°CA AFTDC]	−6.00
Diesel fuel main duration [°CA]	6.85
Diesel fuel in pilot injection [mass%]	14.90
Diesel fuel in pre-injection [mass%]	18.40
Diesel fuel in main injection [mass%]	66.70
Residuals [mass%]	10
EGR [mass%]	0
Swirl ratio [-]	1.8

**Figure 2.** Comparison between the experimental and numerical results (a). Comparison between the Natural gas-Diesel and Biogas-diesel numerical results (b).**Table 5.** Base operating points.

	NG	BG
Engine speed [rpm]	3000	3000
BMEP (brake torque) [bar (Nm)]	8 (177)	8 (177)
Power [kW]	55.6	55.6
Diesel fuel mass [mg/cycle/cyl]	7.60	7.60
CH <sub>4</sub> mass [mg/cycle/cyl]	24.25	25.26
Air mass [mg/cycle/cyl]	765.22	739.13

#### 2.4. Combustion System Design Criteria

As previously mentioned, the development of a new combustion system for DF combustion centered around optimizing the design of both the piston bowl geometry and the injector tip while the cylinder head remains flat, just like the original engine. The bowl shape was assumed to be cylinder-shaped with a rounded bottom. The perfect axial symmetry of the combustion chamber design, including the six-hole injector nozzle, allowed for the use of a 60° sector mesh, which was the same mesh employed in the diesel engine simulations. The most relevant geometric parameter analyzed in the study was the piston bowl radius, which varied from 23 to 38 mm in steps of 5 mm (4 cases), while the bowl

depth was adjusted to maintain the same compression ratio of the reference engine. As a secondary geometric parameter, the radius of the bottom edge of the bowl was considered, where the analyzed values were 3, 5 and 8 mm. Figure 3 shows the new combustion chambers in comparison to the original one, while Table 6 reviews their main features. Each geometry was identified by 2 numbers: the first was the bowl radius (in millimeters), while the second, preceded by “R”, was the bottom edge radius (in millimeters). As an example, “23R3” means that the radius of the cylindrical bowl was 23 mm, while the radius of the bottom edge was 3 mm.

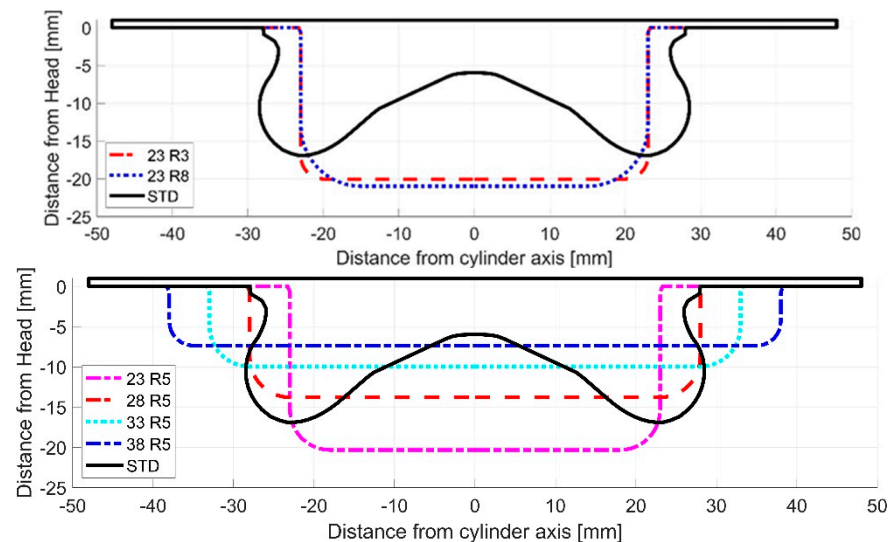


**Figure 3.** Bowl geometries.

**Table 6.** Details of the analyzed combustion systems.

Name	Bowl Radius [mm]	Bottom Edge Radius [mm]	Bowl Depth [mm]	Nozzle Offset [mm]	Tilt Angle [°]
Ref. engine	28.00	–	6.04–16.86	3	75
23R3	23.00	3.00	20.05	2–10	30–120
23R5	23.00	5.00	20.35	2–10	30–120
23R8	23.00	8.00	21.00	2–10	30–120
28R5	28.00	5.00	13.80	2–10	30–120
33R5	33.00	5.00	9.97	2–7	30–120
38R5	38.00	5.00	7.55	2–4	30–120

As far as the injector nozzle is concerned, for each design of the bowl, two parameters were considered: the distance along the cylinder axis from the injector hole to the cylinder head (nozzle offset) and the tilt angle, i.e., the angle formed by the spray axis with the cylinder axis (see Figure 4). The first parameter was varied from 2 to 10 mm (in steps of 1 mm) and the second from 30° to 120° (in steps of 15°). A minimum clearance of 3 mm between the piston and the injector tip was imposed; obviously, the configurations that could not comply with this constraint were discarded.

The computation grid for each geometry was constructed by means of the K3PREP pre-processor with the same criteria used for the base engine mesh: a 60° sector grid was considered, and a typical cell size of 0.8 mm was adopted as for the original mesh. The computational grids of the new combustion chambers are shown Figure 5.

As mentioned in the previous sections, the composition of BF is strongly variable. In this study, the fraction of CH<sub>4</sub> was assumed to be equal to 0.65, which is an average composition that can be easily obtained without major refining while maintaining a good lower heating value.

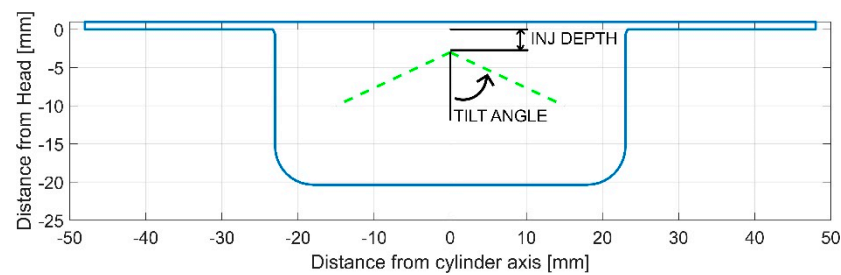


Figure 4. Injector depth and tilt.

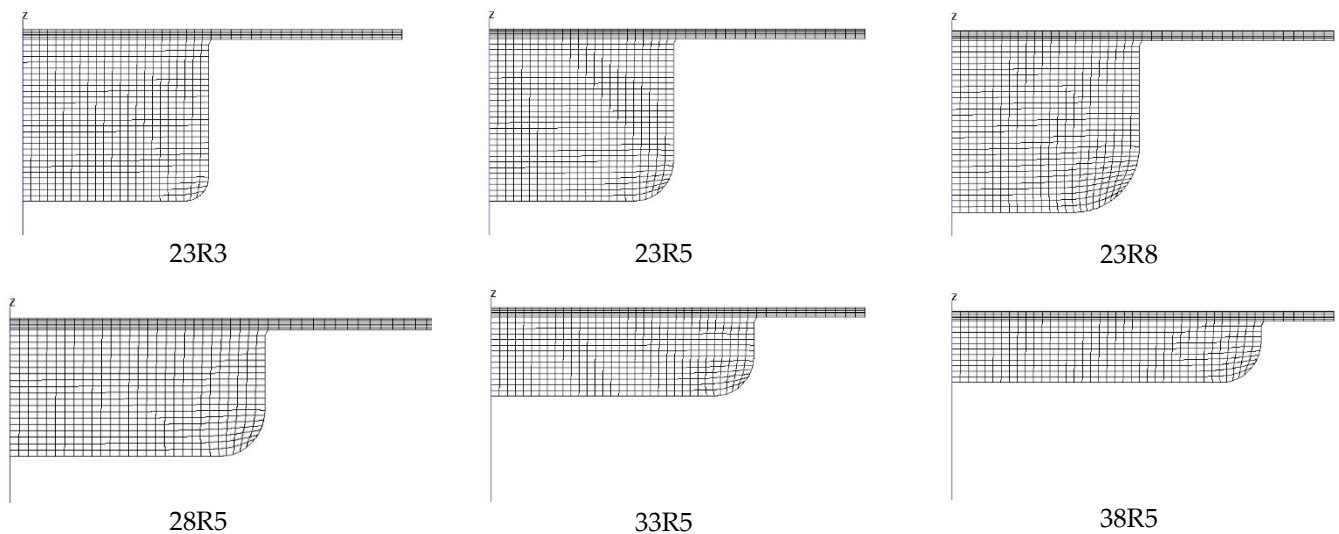


Figure 5. Computational grids of the tested bowls.

The simulations were carried out at two different operating points (Table 7):

- FL: “Full load”—BMEP = 8 bar, brake torque = 177 Nm and engine speed = 3000 rpm. At this operating point, the engine delivered a brake power output of 55.6 kW, corresponding to an electrical power of about 50 kW, which is the limit for micro-generation.
- PL: “Partial Load”—BMEP = 4 bar and engine speed = 3000 rpm (50% of maximum load). To achieve this target, the fuel rate needed to be reduced by 40%. The air/fuel ratio increased from 22 to approximately 31.

Table 7. Full load and partial load initial conditions.

	Total Mass [mg]	O <sub>2</sub> [mg]	Diesel Fuel [mg]	CH <sub>4</sub> [mg]	(A/F) Premix [-]	(A/F) Tot [-]
FL	830.567	170.0	7.60	25.66	28.81	22.23
PL	663.54	139.1	4.50	14.71	41.10	31.47

### 3. Results and Discussion

In this section, the results of the combustion simulations carried out for the optimization of the piston bowl geometry and the injector tip are presented and discussed. As already mentioned, the goal of the optimization was to identify a configuration that yielded a good trade-off between thermal efficiency and NO<sub>x</sub> emissions at both full and partial loads. The other pollutant emissions (soot, HC, CO) were not considered in the design because they were very low (soot) or easily handled by a standard oxidation catalyst (HC and CO).

The first phase of the simulations was carried out at peak power (BMEP = 8 bar, engine speed = 3000 rpm, brake power = 55.6 kW) with the same injection strategy for all the cases. The strategy was defined on the basis of the experimental campaign carried out on a very similar version of the DF engine running on NG and diesel fuel with the standard diesel bowl [44].

The results of the first set of simulations did not permit identifying a single configuration that was better than the original design. The reasons were as follows: first, the diesel bowl worked quite well at full load thanks to the experimental calibration; second, the diesel fuel injection strategy could not be optimized for all the alternative bowls due to the limits of the computational resources. However, the most promising designs for the bowl and the injector tip were identified for further simulations. These configurations were examined in the second round and were carried out at partial load. Here, the diesel injection strategy was optimized for each configuration. The injection pattern optimization was based on a design of experiment (DOE) in which the SOI was shifted from the original one in a range of  $-7$  °CA to  $+5$  °CA (in steps of 2 °CA). Finally, the best combustion chamber design at partial load was simulated at full load, with further optimization of the injection strategy.

### 3.1. Analysis of Peak Power

To provide an overview of the most relevant results of this first round of simulations, a  $\text{NO}_x$ -indicated mean effective pressure (IMEP) diagram was considered. Since the amount of injected fuel was the same, the IMEP was proportional to the indicated thermal efficiency (ITE); therefore, it provided a quite straightforward indication of the BTE. It should be noted that the amount of  $\text{NO}_x$  was expressed as a specific quantity (mass flow rate of incomplete  $\text{NO}_x$  combustion).

Figure 6a focuses on the influence of the piston bowl radius (23, 28, 33 and 38 mm), while the radius of the bowl bottom edge was set at 5 mm. All the signs with the same color refer to the same bowl geometry; the differences were due only to the injector nozzle (see Table 6). The purple star symbol indicates the reference bowl diesel engine.

As expected, most points tended to fall close to the Pareto front since rapid and complete combustion is generally associated with high values of the IMEP and  $\text{NO}_x$  and vice versa.

In order to improve the interpretation of the results, the Y-axis was reversed. In fact, as can be noticed from Figure 6a, the dashed green lines divide the graph into four regions: the optimal region is shown near the origin of the axis since the IMEP was growing and the  $\text{NO}_x$  emissions were lowering with respect to the reference case. Conversely, the worst region is shown in the top-right quadrant where the IMEP was lowering and the  $\text{NO}_x$  emissions were growing.

Figure 6a shows that only the 23R5 bowl improved the thermal efficiency, achieving IMEP values above the base case for a large proportion of the injector setups. Unfortunately, the slight increase in the IMEP was offset by a strong increase in  $\text{NO}_x$ . The best compromise for all the cases was found for a single configuration of the 28R5 bowl, characterized by a nozzle offset of 8 mm and a spray tilt angle of  $90^\circ$  (named 28R5\_90\_8): this setup yielded about the same performance as the original diesel bowl. This outcome was not so surprising, as the new bowl had the same radius as the baseline. It is further confirmation of the paramount importance of this geometric parameter.

When considering the bottom edge radius (Figure 6b), which varied from 3 to 8 mm on the bowl having a radius of 23 mm, it is quite evident that the influence of this parameter was very weak: in fact, the series tended to superpose, at least for high values of the IMEP. Therefore, the parameter seemed not worthy of further investigations, and it was set at 5 mm for the next simulations.

Figure 7 provides information on the influence of the injector, which was characterized by the distance of its tip from the cylinder head and by the tilt angle. For the sake of brevity, only the 23R5 bowl was considered. Figure 7a maps the IMEP as a function of the two

injector parameters, while Figure 7b displays  $\text{NO}_x$  with the same graphical format. In both figures, the red-dotted lines correspond to the values obtained with the original bowl. Figure 7 clearly demonstrates that the tilt angle had a stronger influence than the position of the injector tip. However, between 60 and 105 degrees, the values of the IMEP and  $\text{NO}_x$  did not change very much.

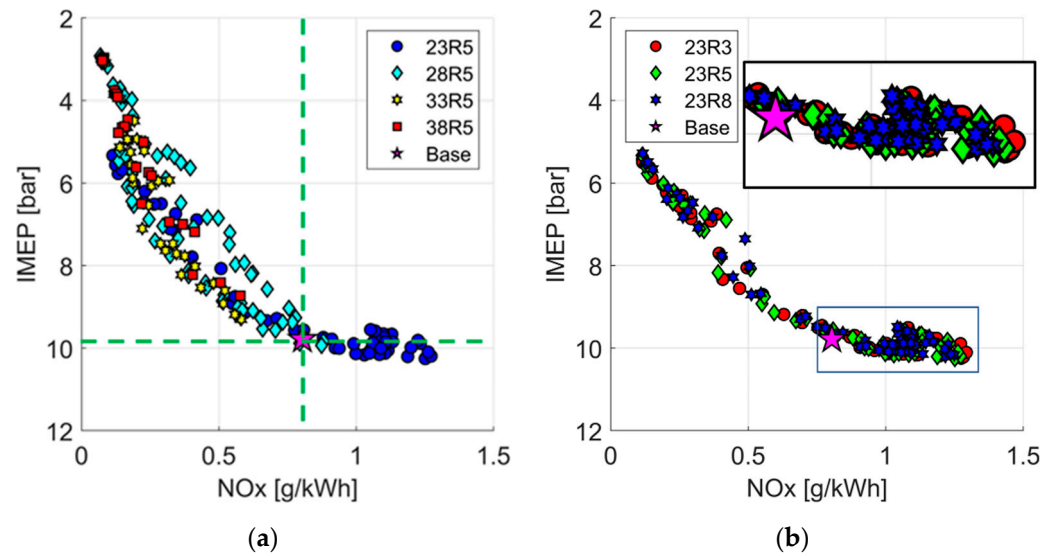


Figure 6. (a) FL with all bowls; (b) FL with a focus on R23.

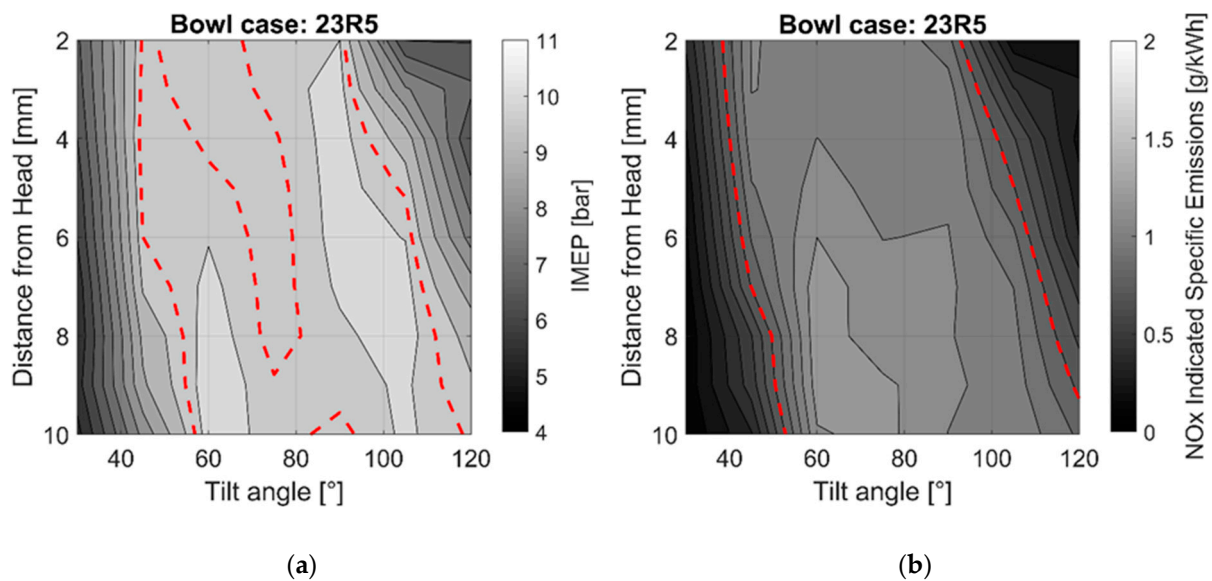


Figure 7. Bowl 23R5 IMEP (a) and a specific  $\text{NO}_x$  plot with standard bowl isolines (b).

In conclusion, the results of the first round of simulations may be summarized as follows:

- At peak power, it was very hard to improve the trade-off between  $\text{NO}_x$  and thermal efficiency provided by the original diesel bowl.
- The diameter of the bowl was the most sensitive parameter, where deeper bowls characterized by a short radius seemed more efficient; this advantage became relevant at partial load, where the combustion tended to be incomplete in the original bowl.
- The position of the injector tip along the cylinder axis seemed less relevant than the tilt angle; however, there was a wide range for the last parameter, whereas the  $\text{NO}_x$  and IMEP remained quite constant.

- There were two promising directions for the development of the combustion system: the first one was the bowl 28R5\_90\_8, which provided the best trade-off between the  $\text{NO}_x$  and IMEP; the second was the 23R5 bowl for different setups of the injector.

### 3.2. Partial Load Analysis

At partial load, the injection strategy played quite an important role, and thus, it must be optimized for each analyzed configuration. For the sake of simplicity, the shape of the diesel fuel injection rate remained constant, as well as the dwell angle between the shots. Only the start of injection (SOI) angle was modified.

The following sweep ranges were chosen:

- The SOI of the main injection pulse varied from  $-7$  to  $+5$  °CA aTDC (in  $2$  °CA steps);
- The injector offset varied from  $4$  to  $10$  mm (in  $1$  mm steps);
- Four injection tilt angles:  $60^\circ$ ,  $75^\circ$ ,  $90^\circ$  and  $105^\circ$ .

The two geometries under investigation were bowl 28R5 and bowl 23R5. However, for the former one, we considered only one injector setup (tilt angle:  $90^\circ$ , injector offset:  $8$  mm).

The first round of simulations at partial load aimed to compare the behavior of the reference bowl to that of bowl 28R5 while sweeping the SOI angle. Figure 8 shows this comparison in terms of the IMEP and specific  $\text{NO}_x$ . It is quite evident that the new bowl did not provide any real advantage in comparison to the original one. Therefore, the attention was focused on the deeper bowl (23R5).

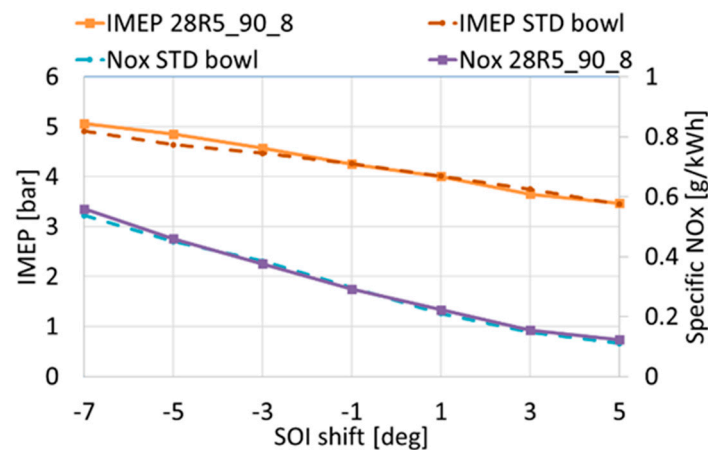


**Figure 8.** Comparison at PL between the standard bowl and 28R5\_90\_8 bowl in terms of the IMEP and specific  $\text{NO}_x$ .

For the sake of clarity, the PL simulation results for the 23R5 bowl, shown in Figure 9, were divided into four plots, with each one corresponding to a single tilt angle ( $a = 60^\circ$ ,  $b = 75^\circ$ ,  $c = 90^\circ$ ,  $d = 105^\circ$ ). The baseline is represented by purple stars.

The results of the analyses can be summarized as follows:

- The best trade-off achieved by the standard bowl appeared to be specific  $\text{NO}_x = 0.5$  g/kWh and IMEP = 4.9 bar.
- There were several new configurations that yielded the same IMEP and lower  $\text{NO}_x$ ; in particular, the configuration with tilt =  $90^\circ$  and offset =  $4$  mm reduced the specific  $\text{NO}_x$  by 38% ( $0.54$  vs.  $0.33$  g/kWh) compared with the baseline at the same IMEP (4.9 bar).
- Accepting a value of the IMEP lower than 4.9 bar, the advantage in terms of  $\text{NO}_x$  of the new bowl design at partial load became larger, but a penalization at full load was expected.
- Accepting values of  $\text{NO}_x$  higher than  $0.5$  g/kWh, the new design of the bowl was more efficient, as it could provide values of the IMEP up to 6 bar (20% higher than the baseline);

- The optimization of SOI led to the following final configurations: STD bowl (SOI  $-7^{\circ}$  CA aTDC), 23R5\_90\_4 (SOI  $-1^{\circ}$  CA aTDC) and 28R5\_90\_8 (SOI  $-5^{\circ}$  CA aTDC).

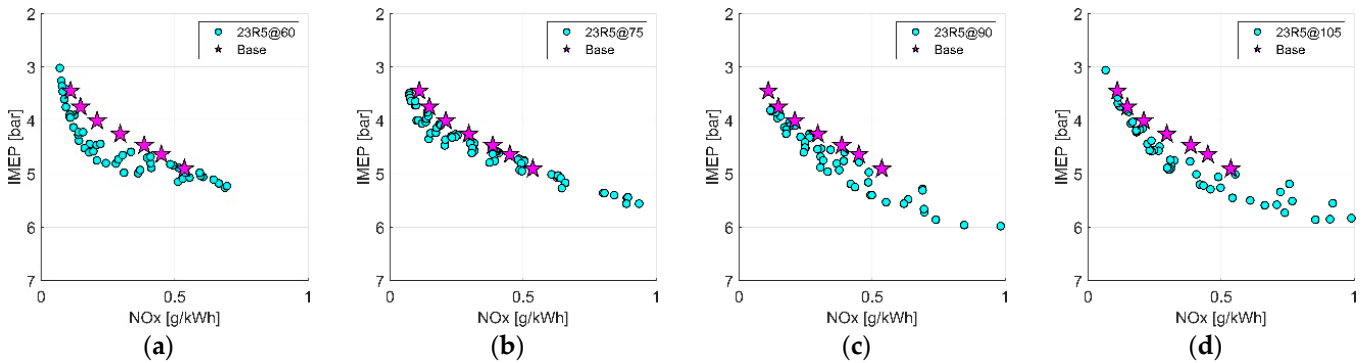
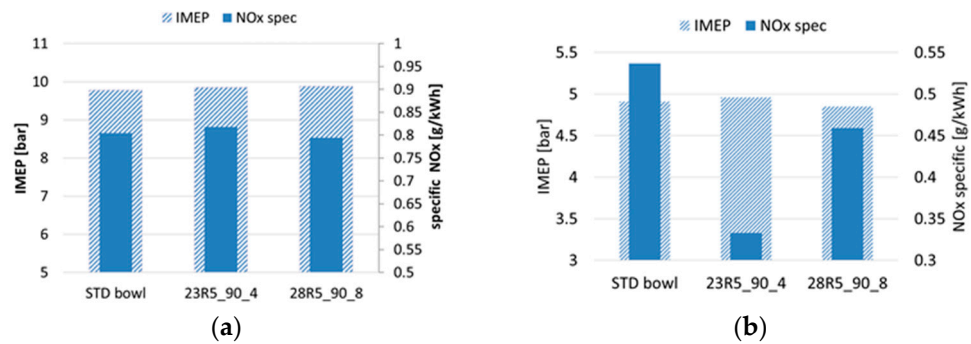


**Figure 9.** Comparison at PL between the standard bowl (purple stars) and the 23R5 bowl (cyan circles) in terms of varying the tilt angle, depth and SOI. Tilt: 60 deg (a); 75 deg (b); 90 deg (c); 105 deg (d).

### 3.3. Final Optimization

In this section, two more promising configurations at PL (23R5\_90\_4 and 28R5\_90\_8) were further investigated and compared with the original geometry (STD bowl).

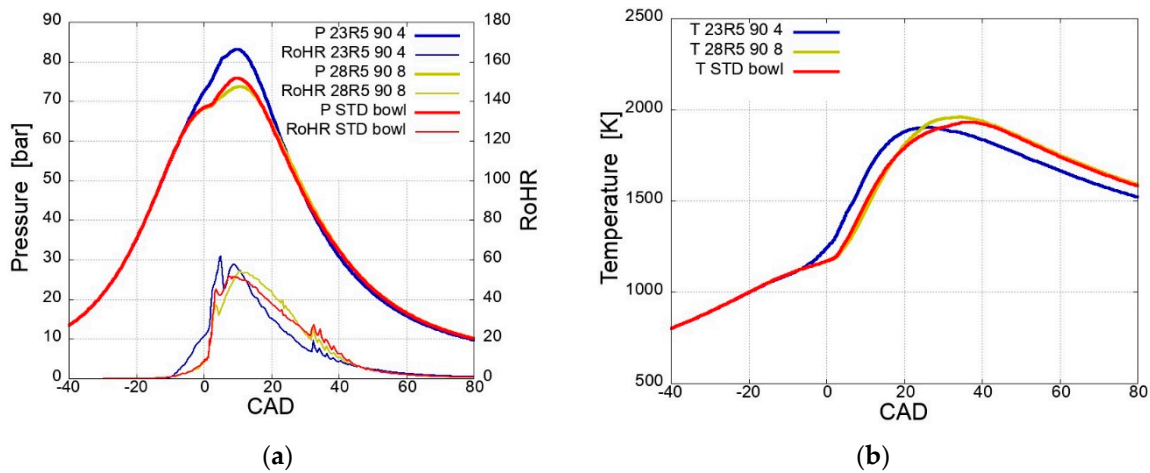
First, it was observed that the original injection strategy at FL of 23R5\_90\_4 led to higher values of both the IMEP and NO<sub>x</sub> than the STD bowl (see Figure 10a); with the specific tuning of the injection parameters, it was possible to reduce both the IMEP and NO<sub>x</sub> emissions to find a new trade-off that was almost perfectly equivalent to the base engine.



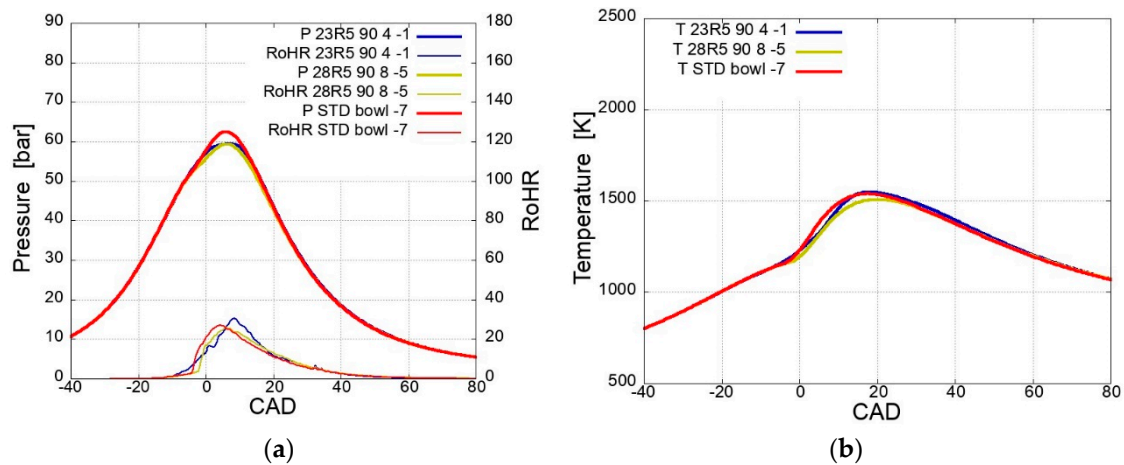
**Figure 10.** Comparison between the bowls at full load (a) and partial load (b): IMEP and NO<sub>x</sub> emissions.

Figure 10 shows a comparison between the 23R5\_90\_4 (with optimized injection strategy), 28R5\_90\_8 and STD bowls. At FL, the IMEP and NO<sub>x</sub> were almost the same; however, at PL, the NO<sub>x</sub> emissions were reduced by 14.5% (28R5) and 38% (23R5) with equivalent IMEPs.

For a more detailed insight into the combustion process, Figures 11 and 12 present the traces of the in-cylinder pressure, temperature and rate of heat release (RoHR) at both full and partial loads. At FL, the behavior of 28R5 was very similar to that of the diesel geometry, while 23R5 generated a higher pressure peak. This was due to the stronger contribution of the pilot injections, which burned before the TDC, to the increase in the RoHR. Probably, the 23R5 design tended to reduce the diffusion of the diesel fuel jets, favoring the local formation of the ignitable mixture before the TDC. However, Figure 11b also shows that the higher peak pressure did not correspond to a higher peak temperature; for this reason, the final NO<sub>x</sub> values were comparable.



**Figure 11.** In-cylinder pressure and rate of heat release (a) and temperature (b) at FL (BMEP = 8 bar, 3000 rpm).



**Figure 12.** In-cylinder pressure and rate of heat release (a) and temperature (b) at PL (BMEP = 4 bar, 3000 rpm).

The situation was different at PL: the advantage in terms of  $\text{NO}_x$  provided by the new bowl could not be explained in terms of the peak cylinder temperature, which was almost equivalent, as shown in Figure 12b. It should be noted that the cylinder temperature was an average parameter, while the formation of  $\text{NO}_x$  was controlled by the local temperature. Therefore, Figure 13 shows a temperature map plotted on a radial cross-section at the crank angle corresponding to the peak of average temperature ( $18^\circ$  aTDC). Here, it is evident that the region at high local temperatures (depicted in yellow and red) was much smaller for 23R5. It may be concluded that the reduction of  $\text{NO}_x$  at PL provided by 23R5 was related to a more uniform distribution of the local temperature, limiting the formation rate of the pollutant.

As a general conclusion, for a DF engine running on diesel fuel and BG, the standard design of the piston bowl yielded a near-optimal trade-off at full load between the thermodynamic efficiency and pollutant emissions; however, at partial load, significant advantages were found by designing a deeper cylindrical bowl with a smaller radius.

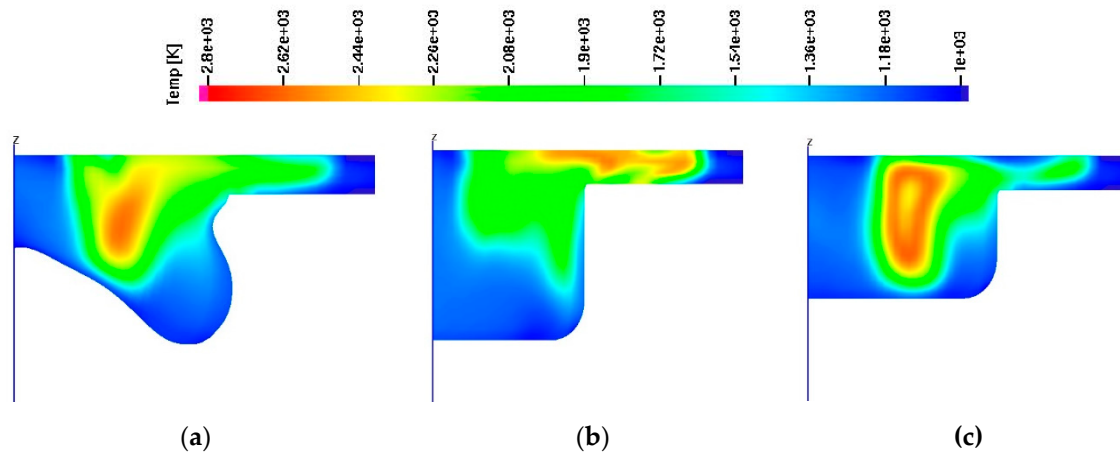


**Figure 13.** Temperature distribution at PL in the following configurations: STD (a), 23R5 (b) and 28R5 (c).

In conclusion, the best configuration found with respect to the standard diesel bowl geometry at partial load was the 23R5\_90\_4, which was a cylindrical-shaped bowl characterized by a 23 mm radius, 5 mm bottom edge radius, 90° injection tilt angle, 4 mm injector tip depth and  $-1^\circ\text{CA}$  SOI.

#### 4. Conclusions

This study explored, by means of 3D CFD simulations, the influence of the combustion chamber design on the performance and emissions of a DF BG–diesel fuel engine for micro-cogeneration applications (maximum electric power: 50 kW). The main engine characteristics were defined in a previous study, where an automotive light-duty diesel engine was modified to run on BG composed of 65% methane while maintaining the original combustion chamber and injector. The aim of the current study was to improve the trade-off between the BTE and  $\text{NO}_x$  emissions, considering both full and partial loads.

The simulations were carried out using a customized version of the KIVA3V software. The numerical model was previously calibrated by the authors on the basis of an experimental campaign carried out on a DF version of the engine adopting a standard diesel piston bowl.

At full load (3000 rpm, BMEP = 8 bar, brake thermal power = 55.6 kW), four different cylindrical bowl shapes were tested, with the bowl radius varying from 23 to 33 mm, while the radius of the bottom edge could be 3, 5 or 8 mm; the bowl depth was adjusted in order to maintain the same compression ratio. The influence of the injector tip position and the spray tilt angle were numerically analyzed by varying the former from 2 to 10 mm and the latter from 30 to 120 deg. A comparison with the original geometry was made by means of a Pareto chart of the IMEP and specific  $\text{NO}_x$  emissions.

At full load, while maintaining the same injection strategy for all the cases, the new bowls did not provide any relevant advantage in terms of the trade-off between the IMEP and  $\text{NO}_x$ : the only configuration that was slightly better than the original one was 28R5 (bowl radius 28 mm, bottom edge radius 5 mm), yielding a +1% IMEP and  $-1.26\%$  specific  $\text{NO}_x$ . However, the deeper bowl (23R5, bowl radius 23 mm, bottom edge radius 5 mm) also appeared very promising since many injector configurations were able to improve the IMEP, and thus, the efficiency of the thermodynamic cycle. With further numerical optimization of the injection strategy, the configuration 23R5 became fully equivalent to the original bowl and the 28R5 bowl.

Finally, the two best designs found at full load (23R5 and 28R5) were tested at partial load (BMEP = 4 bar, 3000 rpm), along with the original bowl. The numerical investigation also included the injection strategy: an SOI range of 12 deg was swept in the simulations.

In comparison to the original bowl, at the same value of the IMEP, 28R5 showed a reduction in specific  $\text{NO}_x$  of 14%, while for 28R5, the improvement was 38%.

**Author Contributions:** Methodology, S.C., A.V., F.S., T.S., E.M. and C.A.R.; software, S.C., A.V., F.S., T.S., E.M. and C.A.R.; validation, S.C., A.V., F.S., T.S., E.M. and C.A.R.; formal analysis, S.C., A.V., F.S., T.S., E.M. and C.A.R.; writing—original draft preparation, S.C., A.V., F.S., T.S., E.M. and C.A.R.; supervision, S.C., A.V., F.S., T.S., E.M. and C.A.R. All authors have read and agreed to the published version of the manuscript.

**Funding:** This research received no external funding.

**Data Availability Statement:** The data presented in this study are available on request from the corresponding author.

**Acknowledgments:** Activity carried out within the project “Decarbonisation of internal combustion engines” was co-financed by the Department of Engineering “Enzo Ferrari” of the University of Modena and Reggio Emilia under the Research Development Plan DIF 2021 2022 (Piano di Sviluppo della Ricerca DIF 2021 2022—FAR Dipartimentale 2021–2022—azione 1)).

**Conflicts of Interest:** The authors declare no conflict of interest.

## Acronyms and Symbols

### Acronyms

A/F	Air-to-fuel ratio [-]
aTDC	After the top dead center
BDC	Bottom dead center
BG	Biogas
BMEP	Brake mean effective pressure [bar]
BTE	Brake thermal efficiency [%]
$\text{C}_2\text{H}_6$	Ethane
$\text{C}_3\text{H}_8$	Propane
$\text{C}_7\text{H}_{16}$	Heptane
$\text{C}_7\text{H}_8$	Toluene
$^\circ\text{CA}$	Crank angle degree [ $^\circ$ ]
CFD	Computational fluid dynamics
$\text{CH}_4$	Methane
CI	Compression ignition
CO	Carbon monoxide
$\text{CO}_2$	Carbon dioxide
CR	Compression ratio
DF	Dual fuel
DI	Direct injection
DME	Dimethyl ether
EGR	Exhaust gas recirculation
EVO	Exhaust valve opening
FL	Full load condition
gISFC	Gross indicated specific fuel consumption [g/kWh]
$\text{H}_2$	Hydrogen
HC	Unburnt hydrocarbon
IDI	Indirect injection
IMEP	Indicated mean effective pressure [bar]
ITE	Indicated thermal efficiency [%]
IVC	Intake valve closing
KH-RT	Kelvin–Helmholtz/Rayleigh–Taylor
$\text{N}_2$	Nitrogen
NG	Natural gas
$\text{NO}_x$	Nitrogen oxides
$\text{O}_2$	Oxygen

Pa SR	Partially stirred reactor
PL	Partial load condition
RCCI	Reactivity-controlled compression ignition
RNG	Renormalization group
RoHR	Rate of heat release
SI	Spark ignition
SOI	Start of injection
TDC	Top dead center
TFC	Turbulent flame closure
Symbols	
$k$	Turbulent kinetic energy [ $\text{m}^2/\text{s}^2$ ]
$\varepsilon$	Dissipation rate of turbulent kinetic energy [ $\text{m}^2/\text{s}^3$ ]
$l$	Maximum distance traveled by the flame front [m]
$h$	Bowl depth [m]
$d$	Bowl diameter [m]
$V_{\text{bowl}}$	Bowl volume [ $\text{m}^3$ ]

## References

- Augustyn, G.; Mikulik, J.; Rumin, R.; Szyba, M. Energy Self-Sufficient Livestock Farm as the Example of Agricultural Hybrid Off-Grid System. *Energies* **2021**, *14*, 7041. [\[CrossRef\]](#)
- Alonso-Fariñas, B.; Oliva, A.; Rodríguez-Galán, M.; Esposito, G.; García-Martín, J.F.; Rodríguez-Gutiérrez, G.; Serrano, A.; Feroso, F.G. Environmental Assessment of Olive Mill Solid Waste Valorization via Anaerobic Digestion Versus Olive Pomace Oil Extraction. *Processes* **2020**, *8*, 626. [\[CrossRef\]](#)
- Havrysh, V.; Kalinichenko, A.; Pysarenko, P.; Samojlik, M. Sunflower Residues-Based Biorefinery: Circular Economy Indicators. *Processes* **2023**, *11*, 630. [\[CrossRef\]](#)
- Kalinichenko, A.; Havrysh, V.; Atamanyuk, I. The Acceptable Alternative Vehicle Fuel Price. *Energies* **2019**, *12*, 3889. [\[CrossRef\]](#)
- Legrottaglie, F.; Mattarelli, E.; Rinaldini, C.A.; Scignoli, F. Application to micro-cogeneration of an innovative dual fuel compression ignition engine running on biogas. *Int. J. Thermofluids* **2021**, *10*, 100093. [\[CrossRef\]](#)
- Valenti, F.; Zhong, Y.; Sun, M.; Porto, S.M.; Toscano, A.; Dale, B.E.; Sibilla, F.; Liao, W. Anaerobic co-digestion of multiple agricultural residues to enhance biogas production in southern Italy. *Waste Manag.* **2018**, *78*, 151–157. [\[CrossRef\]](#)
- Sahoo, B.B.; Sahoo, N.; Saha, U.K. Effect of engine parameters and type of gaseous fuel on the performance of dual-fuel gas diesel engines—A critical review. *Renew. Sustain. Energy Rev.* **2009**, *13*, 1151–1184. [\[CrossRef\]](#)
- Yoon, S.H.; Lee, C.S. «Experimental investigation on the combustion and exhaust emission characteristics of biogas–biodiesel dual-fuel combustion in a CI engine. *Fuel Process. Technol.* **2011**, *92*, 992–1000. [\[CrossRef\]](#)
- Giurcan, V.; Movileanu, C.; Musuc, A.M.; Mitu, M. Laminar Burning Velocity of Biogas-Containing Mixtures. A Literature Review. *Processes* **2021**, *9*, 996. [\[CrossRef\]](#)
- Montoya, J.P.G.; Diaz, G.J.A.; Arrieta, A.A.A. Effect of equivalence ratio on knocking tendency in spark ignition engines fueled with fuel blends of biogas, natural gas, propane and hydrogen. *Int. J. Hydrogen Energy* **2018**, *43*, 23041–23049. [\[CrossRef\]](#)
- Porpatham, E.; Ramesh, A.; Nagalingam, B. Investigation on the effect of concentration of methane in biogas when used as a fuel for a spark ignition engine. *Fuel* **2008**, *87*, 1651–1659. [\[CrossRef\]](#)
- Reitz, R.D.; Duraisamy, G. Review of high efficiency and clean reactivity controlled compression ignition (RCCI) combustion in internal combustion engines. *Prog. Energy Combust. Sci.* **2015**, *46*, 12–71. [\[CrossRef\]](#)
- Zhang, Y.; Sagalovich, I.; De Ojeda, W.; Ickes, A.; Wallner, T.; Wickman, D.D. Development of Dual-Fuel Low Temperature Combustion Strategy in a Multi-Cylinder Heavy-Duty Compression Ignition Engine Using Conventional and Alternative Fuels. *SAE Int. J. Engines* **2013**, *6*, 1481–1489. [\[CrossRef\]](#)
- Padala, S.; Woo, C.; Kook, S.; Hawkes, E.R. Ethanol utilisation in a diesel engine using dual-fuelling technology. *Fuel* **2013**, *109*, 597–607. [\[CrossRef\]](#)
- Curran, S.; Hanson, R.; Wagner, R. Effect of E85 on RCCI Performance and Emissions on a Multi-Cylinder Light-Duty Diesel Engine. In Proceedings of the SAE 2012 World Congress & Exhibition, Detroit, MI, USA, 24–26 April 2012; SAE International: Warrendale, PA, USA, 2012. [\[CrossRef\]](#)
- Splitter, D.; Hanson, R.; Kokjohn, S.; Reitz, R.D. Reactivity Controlled Compression Ignition (RCCI) Heavy-Duty Engine Operation at Mid-and High-Loads with Conventional and Alternative Fuels. In Proceedings of the SAE 2011 World Congress & Exhibition, Detroit, MI, USA, 12–14 April 2012; SAE International: Warrendale, PA, USA, 2011. [\[CrossRef\]](#)
- Wei, L.; Geng, P. A review on natural gas/diesel dual fuel combustion, emissions and performance. *Fuel Process. Technol.* **2016**, *142*, 264–278. [\[CrossRef\]](#)
- Nieman, D.E.; Dempsey, A.B.; Reitz, R.D. Heavy-Duty RCCI Operation Using Natural Gas and Diesel. *SAE Int. J. Engines* **2012**, *5*, 270–285. [\[CrossRef\]](#)

19. Zhou, D.Z.; Yang, W.M.; An, H.; Li, J.; Shu, C. A numerical study on RCCI engine fueled by biodiesel/methanol. *Energy Convers. Manag.* **2015**, *89*, 798–807. [[CrossRef](#)]
20. Li, J.; Yang, W.; Zhou, D. Review on the management of RCCI engines. *Renew. Sustain. Energy Rev.* **2017**, *69*, 65–79. [[CrossRef](#)]
21. Mattarelli, E.; Rinaldini, C.A.; Savioli, T.; Scignoli, F. Optimization of a High-Speed Dual-Fuel (Natural Gas-Diesel) Compression Ignition Engine for Gen-sets. *SAE Int. J. Engines* **2021**, *14*, 369–386. [[CrossRef](#)]
22. Cameretti, M.C.; De Robbio, R.; Tuccillo, R. Performance Improvement and Emission Control of a Dual Fuel Operated Diesel Engine. In Proceedings of the 13th International Conference on Engines & Vehicles, Port Jefferson, NY, USA, 10–14 September 2017; SAE International: Warrendale, PA, USA, 2017. [[CrossRef](#)]
23. Liu, J.; Yang, F.; Wang, H.; Ouyang, M. Numerical study of hydrogen addition to DME/CH<sub>4</sub> dual fuel RCCI engine. *Int. J. Hydrogen Energy* **2012**, *37*, 8688–8697. [[CrossRef](#)]
24. Li, Y.; Jia, M.; Liu, Y.; Xie, M. Numerical study on the combustion and emission characteristics of a methanol/diesel reactivity controlled compression ignition (RCCI) engine. *Appl. Energy* **2013**, *106*, 184–197. [[CrossRef](#)]
25. Molina, S.; García, A.; Pastor, J.M.; Belarte, E.; Balloul, I. Operating range extension of RCCI combustion concept from low to full load in a heavy-duty engine. *Appl. Energy* **2015**, *143*, 211–227. [[CrossRef](#)]
26. Dhanalakshmi, C.S.; Kaliappan, S.; Ali, H.M.; Sekar, S.; Depoures, M.V.; Patil, P.P.; Subbaiah, B.S.; Socrates, S.; Birhanu, H.A. Flash Pyrolysis Experiment on *Albizia odoratissima* Biomass under Different Operating Conditions: A Comparative Study on Bio-Oil, Biochar, and Noncondensable Gas Products. *J. Chem.* **2022**, *2022*, 9084029. [[CrossRef](#)]
27. Ali, S.S.; De Poures, M.V.; Damodharan, D.; Gopal, K.; Augustin, V.C.; Swaminathan, M.R. Prediction of emissions and performance of a diesel engine fueled with waste cooking oil and C8 oxygenate blends using response surface methodology. *J. Clean. Prod.* **2022**, *371*, 133323. [[CrossRef](#)]
28. Ramesh, T.; Sathiyagnanam, A.P.; De Poures, M.V.; Murugan, P. Combined Effect of Compression Ratio and Fuel Injection Pressure on CI Engine Equipped with CRDi System Using *Prosopis juliflora* Methyl Ester/Diesel Blends. *Int. J. Chem. Eng.* **2022**, *2022*, 4617664. [[CrossRef](#)]
29. Dempsey, A.B.; Walker, N.R.; Reitz, R.D. Effect of Piston Bowl Geometry on Dual Fuel Reactivity Controlled Compression Ignition (RCCI) in a Light-Duty Engine Operated with Gasoline/Diesel and Methanol/Diesel. *SAE Int. J. Engines* **2013**, *6*, 78–100. [[CrossRef](#)]
30. Gianetti, G.G.; Lucchini, T.; D’Errico, G.; Onorati, A.; Soltic, P. Development and Validation of a CFD Combustion Model for Natural Gas Engines Operating with Different Piston Bowls. *Energies* **2023**, *16*, 971. [[CrossRef](#)]
31. Lee, S.; Park, S. Optimization of the piston bowl geometry and the operating conditions of a gasoline-diesel dual-fuel engine based on a compression ignition engine. *Energy* **2017**, *121*, 433–448. [[CrossRef](#)]
32. Bui, V.G.; Bui, T.M.T.; Hoang, A.T.; Nižetić, S.; Thi, T.X.N.; Vo, A.V. Hydrogen-Enriched Biogas Premixed Charge Combustion and Emissions in Direct Injection and Indirect Injection Diesel Dual Fueled Engines: A Comparative Study. *J. Energy Resour. Technol.* **2021**, *143*, 120907. [[CrossRef](#)]
33. Duc, P.M.; Wattanavichien, K. Study on biogas premixed charge diesel dual fuelled engine. *Energy Convers. Manag.* **2007**, *48*, 2286–2308. [[CrossRef](#)]
34. Prajapati, H.N. Emission analysis of biogas premixed charge diesel dual fuelled engine. *IOSR J. Eng.* **2014**, *4*, 54–60. [[CrossRef](#)]
35. Shimamoto, Y.; Akiyama, K. A study of squish in open combustion chambers of a diesel engine. *JSME* **1970**, *13*, 1096–1103. [[CrossRef](#)]
36. Arcoumanis, C.; Bicen, A.F.; Vafidis, C.; Whitelaw, J.H. Three-Dimensional Flow Field in Four-Stroke Model Engines. *SAE Trans.* **1984**, *93*, 978–987.
37. Amsden, A. *KIVA3V. A Block-Structured KIVA Program for Engines with Vertical or Canted Valves*; Los Alamos National Lab. (LANL): Los Alamos, NM, USA, 1997.
38. Golovitchev, V.I.; Imren, A. *Development of Dual Fuel Combustion Models for Direct Injected Heavy Duty Diesel Engines. Diesel Fuels: Characteristics, Performances and Environmental Impacts*; Nova Publisher: New York, NY, USA, 2013; pp. 85–118.
39. Golovitchev, V.I.; Montorsi, L.; Rinaldini, C.A.; Rosetti, A. CFD Combustion and Emission Formation Modeling for a HSDI Diesel Engine Using Detailed Chemistry. In Proceedings of the ASME 2006 Internal Combustion Engine Division Fall Technical Conference, Sacramento, CA, USA, 5–8 November 2006; pp. 349–358. [[CrossRef](#)]
40. Bogin, G.E.; DeFilippo, A.; Chen, J.Y.; Chin, G.; Luecke, J.; Ratcliff, M.A.; Zigler, B.T.; Dean, A.M. Numerical and Experimental Investigation of *n*-Heptane Autoignition in the Ignition Quality Tester (IQT). *Energy Fuels* **2011**, *25*, 5562–5572. [[CrossRef](#)]
41. Cantore, G.; Mattarelli, E.; Rinaldini, C.A.; Savioli, T.; Scignoli, F. Numerical optimization of the injection strategy on a light duty diesel engine operating in dual fuel (CNG/diesel) mode. *Int. J. Heat Technol.* **2019**, *37*, 682–688. [[CrossRef](#)]
42. Mattarelli, E.; Rinaldini, C.A.; Golovitchev, V.I. CFD-3D analysis of a light duty Dual Fuel (Diesel/Natural Gas) combustion engine. *Energy Procedia* **2014**, *45*, 929–937. [[CrossRef](#)]
43. Scignoli, F.; Vecchio, F.; Legrottaglie, F.; Mattarelli, E.; Rinaldini, C.A. Numerical Investigation of Dual Fuel Combustion on a Compression Ignition Engine Fueled with Hydrogen/Natural Gas Blends. *Fuels* **2022**, *3*, 132–151. [[CrossRef](#)]
44. Legrottaglie, F.; Mattarelli, E.; Rinaldini, C.A.; Savioli, T.; Scignoli, F. Experimental investigation on a diesel engine operated in RCCI combustion mode. *AIP Conf. Proc.* **2019**, *2191*, 020096. [[CrossRef](#)]

**Disclaimer/Publisher's Note:** The statements, opinions and data contained in all publications are solely those of the individual author(s) and contributor(s) and not of MDPI and/or the editor(s). MDPI and/or the editor(s) disclaim responsibility for any injury to people or property resulting from any ideas, methods, instructions or products referred to in the content.